Snow–Ground Interface Temperatures in the Kuparuk River Basin, Arctic Alaska: Measurements and Model

BRIAN TARAS

Solid Solutions, Fairbanks, Alaska

MATTHEW STURM

U.S. Army Cold Regions Research and Engineering Laboratory, Fort Wainwright, Alaska

GLEN E. LISTON

Department of Atmospheric Science, Colorado State University, Fort Collins, Colorado

(Manuscript received 2 October 2001, in final form 14 January 2002)

ABSTRACT

Air and snow–ground interface temperatures were measured during two winters at 33 stations spanning the 180-km-long Kuparuk basin in arctic Alaska. Interface temperatures averaged 7.5°C higher than air temperatures and varied in a manner that was more complex, and on a spatial scale more than 100 times smaller, than the air temperature. Within the basin, two distinct thermal regimes could be identified, with the division at the boundary between coastal and uplands provinces. When each station was classified into one of three snow exposure classes (*exposed, intermediate,* or *sheltered*), accounting for variations in snow depth and thermal properties, 87% of the variation in the average interface temperature could be predicted from air temperature. Individual station interface temperature records were fit using a beta curve that captured the slow decrease in autumn and the rapid rise in spring. Beta curves were specified by three parameters (α, β, and γ) that could be predicted if province and snow exposure class were known. A model based on the beta curves was developed and applied over the basin to predict interface temperatures in both time and space. Tests of the model against data from within the domain and from arctic Alaskan locations outside the domain suggest an accuracy of ± 2°C when simulating average winter interface temperatures, and ± 3°C when simulating daily interface temperatures.

1. Introduction

Arctic Alaska is snow-covered about nine months of the year, and, during most of that time, temperatures at the top and the bottom of the snowpack differ by a substantial amount. In the Kuparuk basin, these differences average more than 7.5°C, and the nature and character of the snow–ground interface temperature field is completely different than that of the air temperature field (Figs. 1a and 1b: data from this study). Beneath the snow, temperatures fluctuate more slowly and with a reduced amplitude as they respond to rapid changes in air temperature and slower changes in the depth and quality of the snow cover.

Local, landscape, and regional gradients in snow cover (Benson 1969; Adams and Roulet 1982; Liston and Sturm 1998; Sturm et al. 2001) produce much of the small-scale spatial variation that is observed in the interface temperature field (Smith 1975; Nelson et al. 1988; Desrochers and Granberg 1988; Sturm and Holmgren 1994). Substantial variations in snow depth and snow properties can occur over distances of a few meters. In contrast, air temperature varies more smoothly and at a spatial scale that is hundreds, perhaps even thousands, of times larger (cf. Figs. 1a and 1b). These dramatic scale differences make prediction of the interface temperature from the air temperature a difficult task.

The prediction scheme can be physically based, empirically based, statistically based, or some combination of the three, but, regardless of which approach is used, local spatial variations in snow depth and properties must be considered. For example, using a physically based model, the snow cover might be evolved layer by layer and the energy balance at the snow surface computed (Anderson 1976; Brun et al. 1989; Jordan 1991). Surface temperature could be projected downward to the soil or biota beneath the snow using heat transfer equations and estimates of snow depth, snow layer structure, and thermal properties. Where continuous mete-

Corresponding author address: Dr. Matthew Sturm, USA-CRREL-Alaska, P.O. Box 35170, Fort Wainwright, AK 99703-0170.
E-mail: Msturm@crrel.usace.army.mil

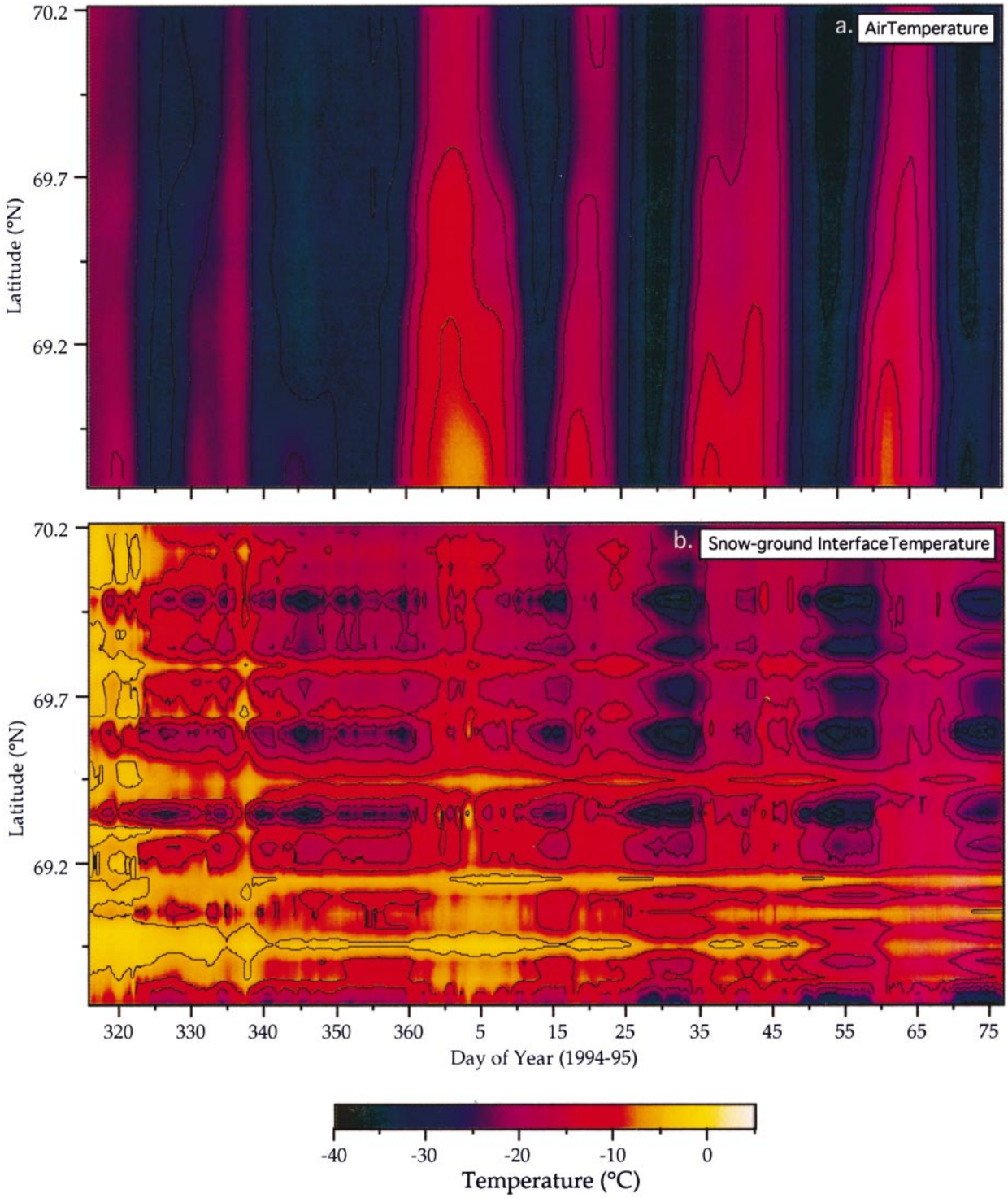

FIG. 1. Kuparuk basin (a) air temperature and (b) snow–ground interface temperature data from this study plotted by latitude and time. Compared to air temperature, the interface temperature is less coherent spatially (thus the horizontal banding) because of landscape-scale variations in snow depth, but is more coherent temporally (horizontal bands are fairly homogeneous) due to the damping effect of the snowpack on air temperature fluctuations.

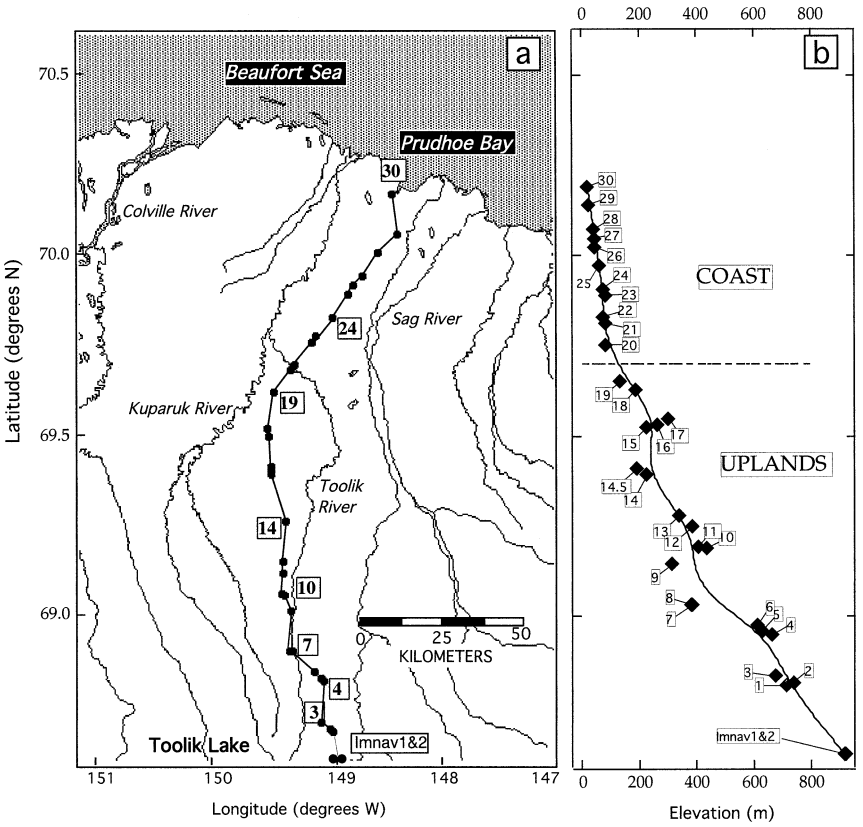

FIG. 2. (a) The Kuparuk River basin showing the locations of the 33 stations where air and snow–ground interface temperatures were recorded. (b) The elevation profile along the line defined by the 33 stations.

orological data are available, this model is likely to produce accurate estimates of snow depth and snow properties, but, with increasing distance from a meteorological station, the quality of the estimates are likely to deteriorate rapidly. Even if the model has the correct physics, if driven with erroneous snow depths, the predicted interface temperatures will be wrong. This problem is particularly acute in the Arctic where the number of meteorological stations is low (IASH 2001).

The same problem of spatial heterogeneity plagues both empirical and statistical models. Ultimately, accurate prediction of interface temperatures over a large domain is going to require understanding of the causes of local spatial variations in snow depth, and developing methods of modeling these variations physically or statistically. For now, however, quantifying the pattern of variation is an important first step. Here, we identify patterns from an extensive set of paired interface and air temperature records collected between 1994 and 1996 at 33 locations across the Kuparuk River basin in arctic Alaska. Inasmuch as the interface temperature is largely controlled by the snow depth, and the depth varies with the landscape (Adams and Roulet 1982; Benson and Sturm 1993; Pomeroy and Gray 1995; König and Sturm 1998; Liston and Sturm 1998), we are able to establish statistical relationships that allow us to predict the interface temperature from landscape characteristics and the air temperature alone. Using our model, we map interface temperatures over a 20 000-km^2 domain in arctic Alaska that includes the 8140-km^2 Kuparuk basin. Like physically based models, our model still requires input data over the entire domain, but far fewer variables need to be extrapolated or interpolated. Moreover, our approach is computationally simpler. Because the primary limitation on prediction accuracy for both physical and statistical models is the quality of the input data, not the basis of the modeling, we think our method provides an attractive alternative for simulating arctic snow–ground interface temperatures for climatic, ecological, and hydrological purposes.

2. Study area

The Kuparuk River basin, which extends from the foothills of the Brooks Range to the Arctic Ocean (Fig. 2a), has two major physiographic provinces (Wahrhaftig 1965; Nelson et al. 1997; Hinzman et al. 1998): the arctic coastal plain (*coastal*) in the north and an area of rolling hills (*uplands*) in the south. Elevations gradually increase southward across the coastal plain, reach-

TABLE 1. Kuparuk basin station locations and landscape classifications.

Station	Lat (°)	Lon (°)	Elevation (m)*	Province	Physiography	Exposure**
Imnav1	68.616	149.285	915	Uplands	Valley	3
Imnav2	68.616	149.302	910	Uplands	Broad ridge	2
1	68.807	149.017	709	Uplands	Intermediate	2
2	68.815	149.038	735	Uplands	Ridge top	1
3	68.834	149.098	671	Uplands	Intermediate (water track)	3
4	68.949	149.079	658	Uplands	Broad ridge	2
5	68.957	149.103	628	Uplands	Broad ridge	3
6	68.975	149.157	610	Uplands	Ridge, windward slope	2
7	69.032	149.325	378	Uplands	Valley	3
8	69.033	149.336	384	Uplands	Valley (terrace)	2
9	69.145	149.335	311	Uplands	Intermediate (water track)	3
10	69.187	149.385	433	Uplands	Broad ridge	2
11	69.192	149.399	404	Uplands	Gentle hill	2
12	69.250	149.398	381	Uplands	Broad, flat valley	2
13	69.280	149.396	335	Uplands	Broad, flat valley	1
14	69.392	149.381	221	Uplands	Valley	2
14.5	69.408	149.378	191	Uplands	Flat	2
15	69.523	149.493	221	Uplands	Valley bench	3
16	69.530	149.494	259	Uplands	Gentle hill	2
17	69.546	149.494	297	Uplands	Broad ridge	1
18	69.627	149.511	183	Uplands	Ridge top	1
19	69.650	149.520	130	Uplands	Intermediate (terrace, wet)	2
20	69.750	149.475	81	Coast	Flat, wet	2
21	69.812	149.344	79	Coast	Flat, dry	2
22	69.827	149.313	73	Coast	Flat, dry	2
23	69.888	149.184	79	Coast	Flat, dry	2
24	69.905	149.147	72	Coast	Flat, wet—standing water	2
25	69.958	149.018	55	Coast	Flat, dry	2
26	70.023	148.893	41	Coast	Flat, dry	2
27	70.045	148.847	41	Coast	Flat, wet	2
28	70.073	148.779	38	Coast	Flat, wet—standing water	2
29	70.137	148.651	23	Coast	Flat, wet	2
30	70.189	148.492	17	Coast	Flat, wet	2

* Estimated from USGS 1:64 000 topographic maps.
** Exposure rank: 1 = exposed, 2 = intermediate, 3 = sheltered.

ing about 100 m at its southern edge (Fig. 2b). They then rise more rapidly, reaching about 1000 m at the extreme southern edge of the basin. The coastal plain is dominated by wet sedge tundra, oriented thaw lakes, and ice-wedge polygons in alluvial and lacustrine deposits, while the uplands comprise north–south-trending broad ridges, isolated rounded mountains, and wide river valleys covered by riparian dwarf willow and birch (Walker et al. 1980, 1994; Walker 1995, 2002). The entire region is underlain by permafrost.

We measured air and interface temperatures at 33 stations along a north–south transect across the basin (Table 1 and Figs. 2a,b). In the uplands, stations were placed in the main types of terrain, including ridges, valleys, hillsides, and water tracks. On the coastal plain, stations were placed in flat wet and dry tundra areas but not in the limited areas where local relief produces snow drifting or erosion. We classified each station by province (coastal or uplands) and describe the local physiography in Table 1. Because wind is critical in redistributing snow in this region, we further classified the stations as *exposed*, *sheltered*, or *intermediate*, based on the local topography and observations of the effects of the wind on the snow at each station.

3. Methods

Air temperatures were recorded at a height of 1.5 m above the ground using inexpensive miniature dataloggers and thermistors housed in white cans with open bottoms. The cans were attached to iron rods driven into the ground. Interface temperatures were recorded about 0.7 m northwest of each rod using a second thermistor covered by white heat shrink and pinned to the vegetation mat using thin wire clips. In areas where there were tussocks, ground thermistors were positioned half way between the base and tops of the tussocks. Data were collected at 2.4- or 3.2-h intervals and are available at the National Snow and Ice Data Center–Arctic System Science Data Coordination Center (NSIDC–ARCSS; Sturm 2002).

The temperature stations were installed in November 1994 and monitored until November 1996, when all instruments were removed. About half of the stations were still running at that time. Loss of stations and data gaps occurred for a variety of reasons, including equipment damage from foxes and water infiltration. The stations were visited each year in November and April. At these times the snow depth was measured at 0.25-m

TABLE 2. Start and end dates of complete and core winters, 1994–97; ND = no data.

	Start of winter	Start of core winter	End of core winter	End of winter
1994/95				
Whole basin*	8 Sep	14 Jan	29 Mar	11 May
Uplands*	8 Sep	18 Jan	31 Mar	6 May
Coastal*	8 Sep	7 Jan	27 Mar	24 May
1995/96				
Whole basin	28 Sep	ND	ND	14 May
Uplands	28 Sep	30 Jan	9 Apr	13 May
Coastal**	28 Sep	ND	ND	24 May
1996/97				
Whole basin	8 Sep	ND	ND	ND
Uplands	8 Sep	ND	ND	ND
Coastal**	7 Sep	ND	ND	ND

* Winter start based on Imnavait stations only.

** Data from one station only for end of 1995/96 winter and start of 1996/97 winter.

TABLE 3. Average interface (T_i) and air (T_a) temperature by province for the Kuparuk basin, 1994–96.

	Complete winter		Core winter	
	T_i (°C)	T_a (°C)	T_i (°C)	T_a (°C)
1994/95				
Whole basin	−12.8	−20.3	−16.2	−25.3
Uplands	−11.9	−19.7	−14.3	−23.7
Coastal	−15.5	−22.1	−19.6	−28.5
1995/96*				
Uplands	−9.6	−17.1	−11.8	−19.1

* Due to equipment failures, only uplands stations are available.

intervals along a line beginning at the iron rod and extending 1.5 m to the northwest, bracketing the location where the interface thermistor was buried.

Based on a study by Whiteman et al. (2000), the thermistors and mini dataloggers had an estimated accuracy of ±0.3°C. Due to electronic limitations, they could not record temperatures lower than −37°C. Meteorological instruments not subject to this low-temperature limitation were operated adjacent to mini dataloggers in three locations. Comparisons of truncated and nontruncated records indicate that the truncated records produced a bias in the average winter air temperature (T_a) of 0° to +1.0°C (for complete list of symbols, see appendix A). Using a regression based on the comparison data, we have corrected for this bias. An additional positive bias was present, particularly in the spring, because the inexpensive mounting system allowed reflected light to enter the shelter and warm the air temperature thermistor. When compared to air temperatures measured at the adjacent meteorological sites where standard vented shelters were used, the average air temperature recorded using the inexpensive shelters was 1° ± 0.5°C too high during sunny weather. In the dark months of November through March this bias was zero.

In April 1995, spot measurements of the snow–ground interface temperature were made at 1-m intervals along 100-m lines bracketing select stations. At these eight stations, the interface temperature records from the time of the survey were within 1.5°C of the average of the spot values. These comparisons suggest that our station records adequately represented the local interface temperature fields.

The temperature records (T_i) were used as a proxy to determine the duration that snow covered the ground at each station based on three distinct dates (Table 2): 1) the day the snow cover formed, 2) the day it began to melt (date when meltwater first arrived at the base of the snowpack), and 3) the day it was all gone. The start of winter was defined as the time when T_i dropped consistently below 0°C. The beginning of the melt was defined as the time when T_i rose to 0°C and remained there for several days, indicating that wet snow surrounded the interface thermistor. The last snow was assumed to disappear when T_i rose above 0°C and became roughly coincident with air temperature. The start of melt was a less ambiguous indicator of the end of winter than the complete disappearance of the snow, so we use it here. The period between the start of the melt and the last disappearance of snow was generally less than 11 days.

Because of substantial data gaps, we found it necessary to define a ''core winter'' period in order to allow for interannual comparisons between the winter of 1994/95 and the following winter, which was the only one monitored in its entirety. In 1994, temperature monitoring began in November and ceased at all stations early in the 1996/97 winter season. Core winter was defined as an interval of time equal to 30% of the total winter centered about the time of the minimum interface temperature. The minimum was defined by fitting a beta curve (discussed later) to the interface temperature record and taking its derivative. Core winter typically encompassed 80 days, or approximately 800 measurements.

4. A description of the Kuparuk temperature fields

The average winter air temperature ($\overline{T}_a$: November–May) for the Kuparuk basin sites in 1994/95 was −20.3°C, while the average snow–ground interface temperature ($\overline{T}_i$) was −12.8°C (Table 3 and appendix B). In 1995/96, winter air temperatures at uplands stations were 2.6° higher than they were in 1994/95, but interface temperatures were higher by a commensurate (2.3°C) amount (Table 3). Despite nearly a 3° interannual difference in air temperature, the thermal protection due to the snow cover (~7.5°C) was about the same both years.

Air and interface temperatures showed marked dif-

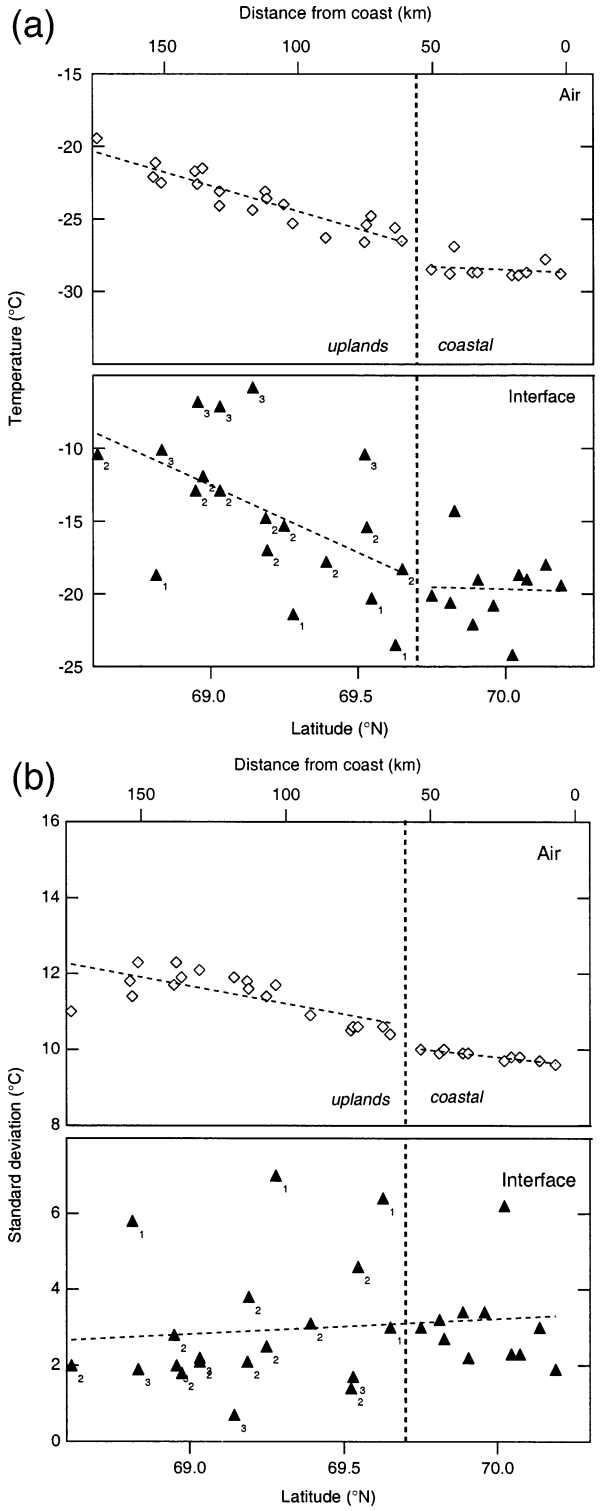

FIG. 3. (a) Average station values of air ($\overline{T}_a$) (open diamonds) and interface temperature ($\overline{T}_i$) (solid triangles) as a function of latitude, showing trends in the uplands and the absence of trends in on the coastal plain, core winter, 1994/95. (b) Average station values of the SD of air temperature (T_a) and the SD of interface temperature (T_i) as a function of latitude, showing trends in the uplands and the absence of trends in on the coastal plain for SD of T_a, but virtually no trends for the SD of T_i. Data is for core winter, 1994/95. Numbers refer to exposure class: 1 = sheltered; 2 = intermediate, 3 = exposed.

ferences between coastal and upland provinces, suggesting some systematic variation in snow cover across the basin. The average air temperature on the coastal plain was 2.4°–4.8°C lower than the average air temperature in the uplands (Table 3: data from complete and core winters of 1994/95, respectively), and the average interface temperature had an even greater offset of 3.6°–5.3°C. Moreover, average values of T_i and T_a, while basically constant across the coastal plain, increased steadily with distance south in the uplands (Fig. 3a). This trend corresponds with both increasing elevation (Fig. 2b) and increasing distance from the coast (Fig. 2a). Trend lines drawn through upland station average air temperatures for 1994/95 (shown in Fig. 3a) and 1995/96 (not shown) have nearly identical slopes, though they are offset by about 3°C due to the higher air temperatures of the second winter. Interface temperatures also showed a distinct slope across the uplands but no slope on the coastal plain. The year-to-year similarity of the slopes suggests that the trends arise from an invariant source, probably the regional topography interacting with weather systems to produce an air temperature lapse rate. In the case of the interface temperature, a second source is the systematic difference in uplands and coastal snow covers: coastal snow was thinner but of more uniform depth (over distances of hundreds of meters) than uplands snow.

Another indication of the systematic difference in the snow cover of the two provinces is the greater spatial variability of interface temperature observed in the uplands than on the coastal plain (Fig. 3a). By considering the exposure class for each station (Fig. 3a, numbers), a reason for the scatter becomes apparent. Interface temperatures were lowest at those sites where the snow was thinnest due to wind erosion (Table 1, class 1), and highest where the snow was deepest due to drifting (Table 1, class 3). With more stations providing a more continuous sampling of snow depth, we suspect that we would have been able to draw a whole family of nearly parallel trend lines, each line incrementally higher or lower, depending on the depth. On the coastal plain, the absence of local relief produced a more uniform snow depth distribution, with eroded or drifted snow limited to only a few places (gullies, cutbanks), which were not sampled.

Temperature fluctuations were smaller at the base of the snow than at the top, reflecting the damping property of the snow. As suggested by Fig. 1 and shown in Fig. 3b, the standard deviation (SD) of T_a at each station was 3–4 times greater than the SD of T_i. For the whole basin, the SD of T_a averaged 11.7°C, while for T_i it averaged only 4.4°C, indicating that the snow reduced air temperature fluctuations by a factor of about 2.5. In

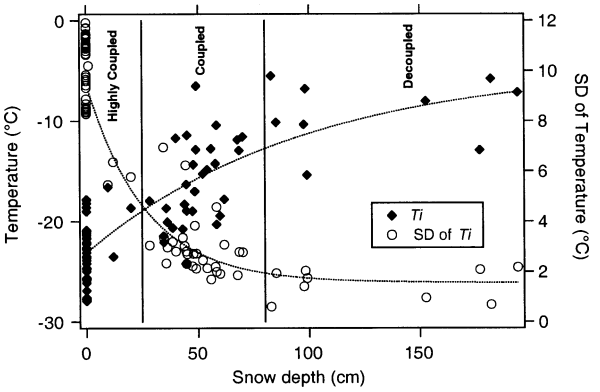

FIG. 4. Coupled and decoupled regimes for the snow–ground interface temperature (T_i) as a function of snow depth.

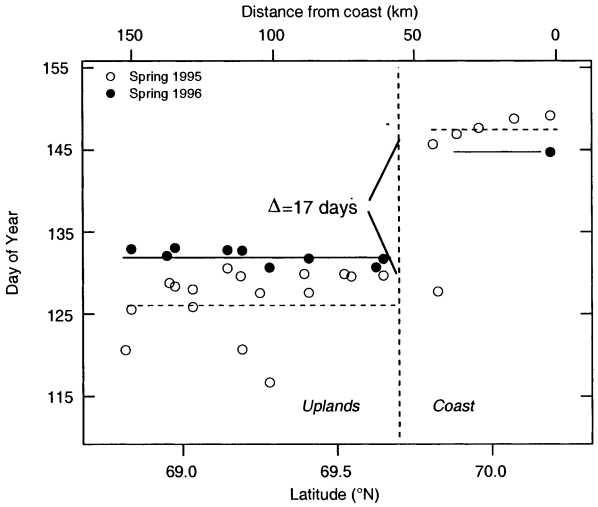

FIG. 5. End of winter, 1995 and 1996, showing the 17-day difference in winter length between the uplands and coastal provinces.

addition, the SD of T_a varied across the basin in a much smoother manner than the SD of T_i (Fig. 3b), reflecting the effect of local variations in snow depth on the latter. As with the air temperature itself, the SD of T_a increased with distance south across the uplands in a nearly linear fashion but was roughly constant across the coastal plain. The SD for T_i, on the other hand, showed no trend, either on the coastal plain or in the uplands. Again, much of the scatter (the SD value) in the interface temperature at each station can be readily explained by exposure class (numbers in Fig. 3b), with deeper snow producing lower values of SD.

We have assigned a specific range of snow depths to each snow exposure class (Table 1) based on measurements made in April, when the pack was near maximum depth: shallow (<25 cm), intermediate (25–80 cm), and deep (>80 cm). They correspond with the exposed, intermediate, and sheltered classes, respectively. The class divisions reflect our general understanding of tundra snow (Benson and Sturm 1993; Sturm et al. 1995, 2001) and fall close to depth values that would produce the maximum discrimination between classes. The majority (66%) of the stations are of intermediate depth, but that is to be expected because intermediate-depth snow covers most of arctic Alaska.

When station average values of T_i and SD of T_i are plotted as a function of snow depth, we can identify three thermal regimes that correspond with the three depth/exposure classes (Fig. 4). For the deepest snow (>80 cm; sheltered), interface temperatures approach a state where they are virtually independent of snow depth. We call this the *decoupled* regime. In this regime, the interface temperature is controlled largely by the moisture content of the soil, the local ground heat flux, and the early winter air temperature history when the snow pack is shallow. Prediction of T_i from T_a for this regime produces less accurate results than for the more highly coupled regimes. For the shallowest snow (<25 cm; exposed), the interface temperature closely mimics the air temperature, and in the limit of no snow equals it exactly. In this case, T_i is *highly coupled* to T_a as well as snow depth, and prediction is relatively easy. For snow of intermediate depth, T_i is still strongly *coupled* to depth and air temperature, though not as much as in the exposed class. These highly coupled, coupled, and decoupled regimes are also apparent when SD of T_i is plotted against depth (Fig. 4, right axis).

Lastly, distinct differences in the length of the winter season between the uplands and coastal provinces were observed. Winter started approximately the same day (±1 day) in both provinces (Table 2) but ended, on average, 17 days later on the coast (1995: 22 days; 1996: 13 days). We can locate the transition point between the shorter uplands winter and the longer coastal winter with some degree of accuracy (Fig. 5). It coincides with the break in slope between the flat coastal plain and the initial topographic rise of the uplands (Fig. 2b), near where the 100-m contour interval is found on topographic maps.

5. A statistical method of predicting the interface temperature

Here we develop a method of predicting the interface temperature over a large domain like the Kuparuk basin using only air temperature and snow depth as input. Air temperature is relatively easy to extrapolate over the domain, but snow depth is not. We avoid this problem by using two categorical variables, snow exposure class and province, to capture the essential dependence of interface temperature on snow depth and snow quality. These can be determined from maps.

The model has two parts. In part 1 we derive, for a location of interest, a smooth curve that describes the seasonal trend of snow–ground interface temperature. In part 2 we add hourly temperature fluctuations to the smooth curve. These fluctuations are important because extreme temperatures and the cycling of temperature can

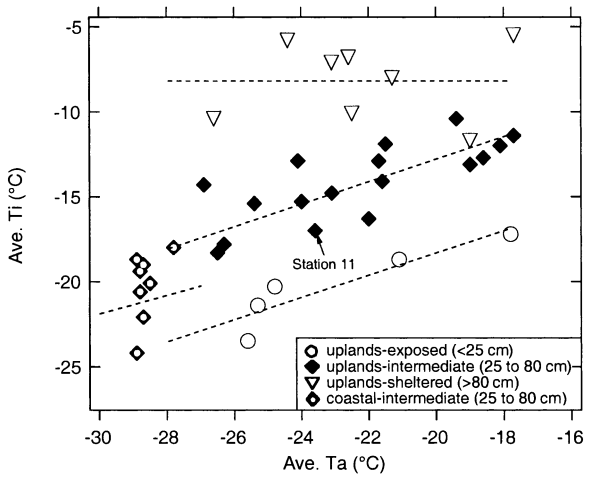

FIG. 6. Average values of interface temperature (T_i) as a function of average air temperature values (T_a), core winters, 1994–96. Separate lines have been fit to each province–exposure class combination separately.

have a greater impact on biophysical systems than the average temperature. The hourly fluctuations are derived from air temperature fluctuations and are damped, more or less, depending on the province and the snow exposure class. In nature, the propagation of air temperature into a snowpack also results in phase shift (time lag). The model incorporates seasonal phase shift, but not phase shifts of higher (daily, hourly) frequency.

a. Part 1

For a given location, the average winter interface temperature $\overline{T}_i$ can be predicted from the average winter air temperature $\overline{T}_a$ using a linear regression model, as long as the province and snow exposure class are also considered (Fig. 6). Due to gaps in the data, we developed regressions using $\overline{T}_{a,\text{core}}$ and $\overline{T}_{i,\text{core}}$, the data for the core winter, rather than data for the entire winter (Table 2 and appendix B). To calculate $\overline{T}_{a,\text{core}}$ from the air temperature record, it is convenient to nondimensionalize time first, so that the complete winter runs from $t = 0$ (beginning) to $t = 1$ (end). Core winter was defined (see section 3) as the period $0.55 \leq t^* \leq 0.85$ for the uplands province and the period $0.47 \leq t^* \leq 0.77$ for the coastal province.

Using province, snow exposure class, and $\overline{T}_{a,\text{core}}$ as input, the predicted average interface temperature, $\overline{T}_{i,\text{core}}$, was computed using an analysis of covariance model (ANCOVA; Neter et al. 1990) (Table 4, relationship 1). Importantly, an F test indicated that the data supported (with 95% confidence) the unique slopes for each province/class listed in the table and shown in Fig. 6. Relationship 1 has a residual standard error of 1.7°C and can be used to predict average winter interface temperature to ±2°C (1σ).

For the uplands province, sheltered class, the ANCOVA indicated a slope that was not significantly different than zero. This is consistent with our finding that T_i is decoupled from snow depth for sheltered snow (Fig. 4). For coastal exposed and sheltered classes, we have no data on which to assign a and b values for relationship 1 (Table 4), but we assume that these classes are similar in behavior to their upland counterparts. Because T_a is lower on the coastal plain than in the uplands (Table 3), and because the coastal intermediate regression line differs from the upland line by about 2.5°C (Fig. 6), we have offset the uplands sheltered equation by −2.5°C. We also offset the uplands exposed equation by a similar amount. Only 31% of the variability of the average interface temperatures shown in Fig. 6 can be explained using average air temperature alone, but, with the addition of province and exposure class as explanatory variables, r^2 increases to 87%.

In order to predict daily or hourly interface temperatures rather than winter average values, a beta curve must be generated for each location of interest. To develop province and class-specific beta curves, we fit a beta curve to each individual station record, determining three fitting parameters, α, β, and γ, using a least squares approach. The shape of the beta curve is determined by α and β. They describe when, during the winter, the minimum interface temperature will occur and how quickly the temperature will drop in the fall and rise in the spring. The temperature scale parameter, γ, normalizes the curve so the area under it equals 1 (a necessary property of beta distributions). Essentially, γ is the negative of the average interface temperature, $\overline{Ti}$. For each fitted curve, we also calculated the mode (M) and the skew (S) (Evans et al. 1993):

$$M = \left(\frac{\alpha - 1}{\alpha + \beta - 2}\right), \tag{1}$$

$$S = \frac{2(\beta - \alpha)(\alpha + \beta + 1)^{0.5}}{(\alpha + \beta + 2)(\alpha\beta)^{0.5}}. \tag{2}$$

The mode varies from 0 to 1 and describes, in nondimensional time (t^*), when the minimum temperature occurs during the winter.

Using the set of all α, β, and γ values generated from the data, we then derived (using regression and ANCOVA models) a series of linked relationships (Table 4, relationships 2, 3, and 4) that predict γ, M, and S. An F test did not support the use of exposure class (a proxy for snow depth) as an explanatory variable in relationship 3. In addition, individual slopes for each province were not supported by the data.

With predicted values of $\hat{\gamma}$, $\hat{M}$, and $\hat{S}$, Eqs. (1) and (2) can be solved for $\hat{\alpha}$ and $\hat{\beta}$, the predicted snow–ground interface beta-curve parameters. With these parameters, a smooth, seasonal interface temperature record $[\hat{\theta}_i(t^*)]$ (Figs. 7c,e) could be computed using the definition of the beta curve (Evans et al. 1993):

TABLE 4. Model ANCOVA and regression statistics by province and exposure class.

		Parameter estimates	Uplands exposed	Uplands intermediate	Uplands sheltered	Coastal exposed[a]	Coastal intermediate	Coastal sheltered[a]	r^2	Residual standard error (°C)	Overall F test (p value)	Model selection F test (p value)
Model-Part 1												
1. ANCOVA	$\hat{\overline{T}}_{i,\text{core}} = a + b\overline{T}_{a,\text{core}}$	a	−5.25	0.49	−8.18	−7.75	−5.07	−10.68	0.87	1.7	<0.0001	0.005[c]
	↘	b	0.65	0.66	0	0.65	0.53	0				
		p value[b]	0.017	<0.0001	0.739	—	0.12	—				
2. Regression	$\hat{\gamma} = a + b\overline{T}_{i,\text{core}}$	a	−0.04	−0.04	−0.04	−0.04	−0.04	−0.04	0.68	0.89	<0.0001	
	↘	b	−0.72	−0.72	−0.72	−0.72	−0.72	−0.72				
		p value[b]	<0.0001	<0.0001	<0.0001	<0.0001	<0.0001	<0.0001				
3. ANCOVA	$\hat{M} = a + b\gamma$	a	0.76	0.76	0.76	0.70	0.70	0.70	0.44	0.05	0.0005	0.011[d]
	↘	b	−0.01	−0.01	−0.01	−0.01	−0.01	−0.01				
		p value[b]	0.020	0.020	0.020	0.020	0.020	0.020				
4. Regression	$\hat{S} = a + bM$	a	0.80	0.80	0.80	0.80	0.80	0.80	0.84	0.04	<0.0001	
		b	−1.53	−1.53	−1.53	−1.53	−1.53	−1.53				
		p value[b]	<0.0001	<0.0001	<0.0001	<0.0001	<0.0001	<0.0001				
Model-Part 2												
5. ANCOVA	$\hat{\varphi} = a + b\gamma$	a	0.27	0.05	0.03	0.25	0.04	0.02	0.87	0.06	0	0.00001[e]
		b	0.02	0.02	0.02	0.02	0.02	0.02				0.945[f]
		p value[b]	0.011	0.011	0.011	0.011	0.011	0.011				

[a] Parameters for this province/exposure class are estimated as explained in text.
[b] P values are for slope parameter b.
[c] Reject ''same slope hypothesis'' in favor of ''separate slopes for each class.''
[d] Reject ''no province/exposure class variation'' in favor of ''variation by province.''
[e] Reject ''no province/exposure class variation'' in favor of ''variation by province and class.''
[f] Fail to reject ''same slope hypothesis'' in favor of ''separate slopes for each class.''

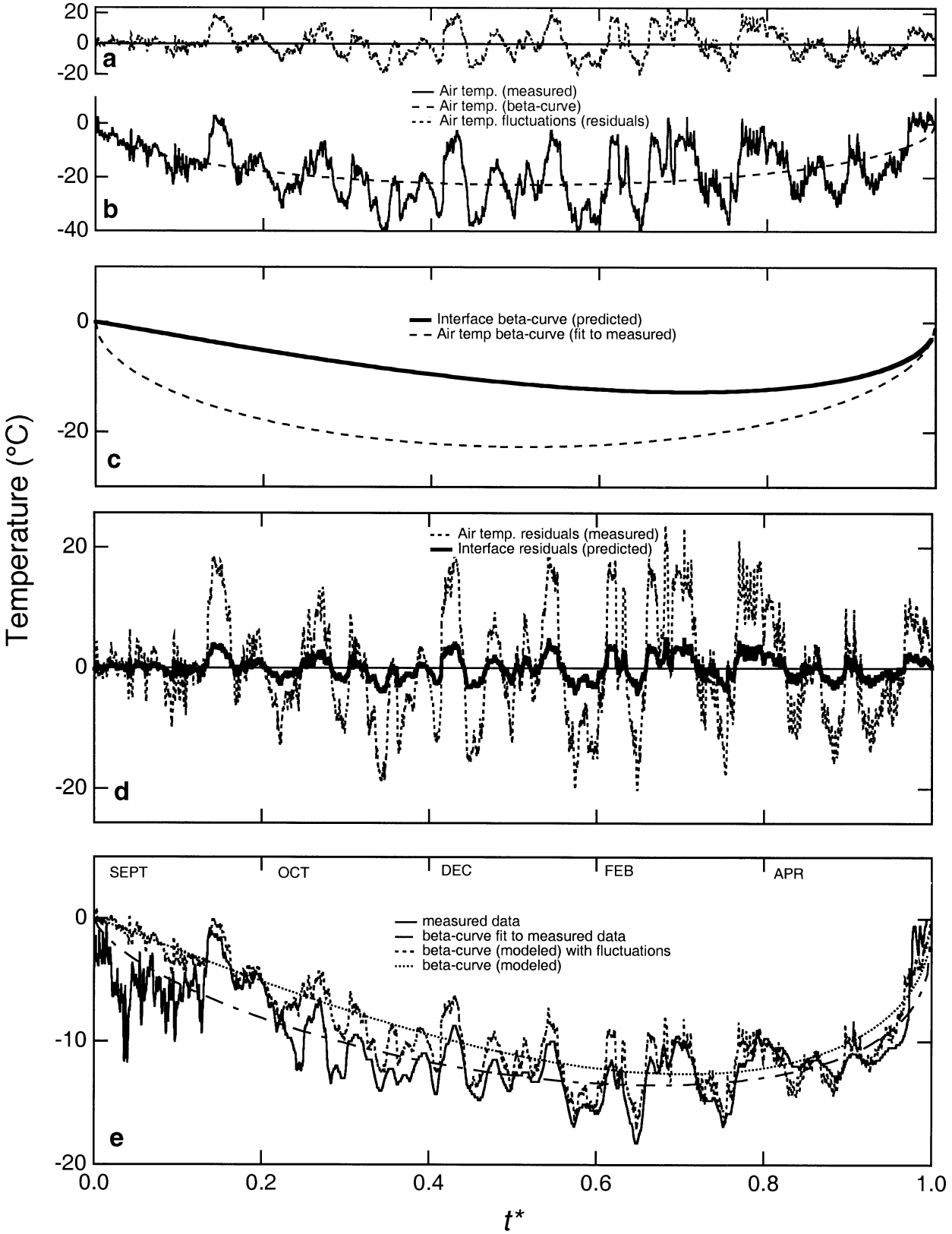

FIG. 7. Air and interface temperature records from station 11, along with beta-fit curves, residuals, and model results. See text for full explanation.

$$\hat{\theta}_i(t^*) = -\hat{\gamma}\left[\frac{\Gamma\{\hat{\alpha}+\hat{\beta}\}}{\Gamma\{\hat{\alpha}\}\Gamma\{\hat{\beta}\}}\right]t^{*(\hat{\alpha}-1)}(1-t^*)^{(\hat{\beta}-1)} \quad (3)$$

for $0 < t^* < 1$, where Γ is the gamma function.

b. Part 2

For many applications, the smooth curve predicted by Eq. (3) would be sufficient, but a more realistic temperature record can be simulated by adding the residual temperature fluctuations to the smooth curve. To do this, fluctuations about a smooth fit to the air temperature record must be computed first. This can be done by fitting the air temperature record for the entire winter with either a beta curve [used here (Fig. 7b): see Eq. (3) for form] or a polynomial. The air temperature residuals (Fig. 7a), $\varepsilon_a(t^*)$, can then be computed from

$$\varepsilon_a(t^*) = T_a(t^*) - \theta_a(t^*) \quad (4)$$

where $T_a(t^*)$ is the measured air temperature, and $\theta_a(t^*)$ is the smooth seasonal curve fit to the measured air temperatures.

The air temperature residuals, $\varepsilon_a(t^*)$, must be damped appropriately (to account for the attenuation of air temperature with depth of the snowpack) for each province and snow exposure class (Fig. 7d). The damping factor (φ) is approximately the observed SD of $T_{i,\text{core}}$ divided by the SD of $T_{a,\text{core}}$:

$$\varphi = \frac{SD_{i,\text{core}}}{SD_{a,\text{core}}}. \quad (5)$$

An ANCOVA model showed that 87% of the variability in the observed damping factor can be explained by γ (recall that γ is the negative of the average interface temperature, $\overline{T}_i$), province, and exposure class (Table 4, relationship 5). An *F* test indicated that the data did not support unique slopes for each province/exposure class combination. Damping factor estimates were then applied to the air temperature residuals [$\varepsilon_a(t^*)$] to produce a damped interface residual, $\hat{\epsilon}_i(t^*) = \hat{\varphi}\varepsilon_a(t^*)$, which was added to the smooth seasonal beta curve [Eq. (3)],

$$\hat{\theta}_{i,\text{resid}}(t^*) = \hat{\theta}_i(t^*) + \hat{\varphi}\varepsilon_a(t^*), \quad (6)$$

to produce a curve with both seasonal and higher-frequency fluctuations.

The modeling procedure (parts 1 and 2) is illustrated in Fig. 7 using data from station 11 (Table 1 and Fig. 2), a station that tended to fall off the various regression lines (see Fig. 6) and provides a reasonably conservative example of model performance. A comparison of the beta curve fitted to the air temperature with the beta curve predicted for the interface temperature (Fig. 7c) shows that the modeling captures the damping effect of the snowpack. It also captures the seasonal shift in timing of the minimum winter temperature, where the mode for the air temperature ($t^* = 0.5$) is shifted more than 30% (to $t^* = 0.67$) at the interface.

A comparison of observed interface temperature records with those predicted by the model shows reasonable agreement. There are two quasi-independent sources of error: 1) a ''seasonal'' error (model, part 1) that arises because the characteristic beta curve for a given province and exposure class does not match exactly the beta curve for the actual station data, and 2) a ''fluctuation'' error (model, part 2) that arises because the predicted damping of the air temperature fluctuations does not match perfectly the actual damping that took place in nature. Combining both sources of error, we estimate model accuracy for daily observations at ± 3°C (1σ).

We have tested the model outside the domain in which it was developed using three air and interface temperature record sets from Ivotuk, a site 200 km west of the Kuparuk basin. These uplands–intermediate and uplands–sheltered sites had average seasonal errors that ranged from 0.9° to 2.5°C and fluctuation errors that ranged from 1.3° to 1.5°C, consistent with our stated error.

6. Model application to the entire Kuparuk basin

Here we simulate the snow–ground interface temperature for the winter of 1994/95 over a 20 000-km^2 rectangular area encompassing the Kuparuk basin using the model described in section 5. For the simulation, we use air temperature records from 6 stations in the domain (Walker 2002) that are completely independent of the 33 air temperature stations used to develop the model. From these 6 stations, a daily average value was assigned to each 100 m $\times$ 100 m grid cell in the domain using linear interpolation/extrapolation and a simple adiabatic lapse rate to adjust for elevation. The uplands–coastal boundary was set to coincide with the 100-m contour from a digital elevation model (DEM; see Hinzman and Kane 2002). Snow exposure class was determined by running a three-dimensional snow-transport model (SnowTran-3D; Liston and Sturm 1998) to produce an end-of-winter snow depth distribution (Liston and Sturm 2002, personal communication), then dividing the continuous depth output from that model into the three depth classes (Fig. 4). The resulting province–class combinations are shown in Fig. 8. For the simulations, we chose 8 September (day 251) as the start of winter, based on the 1994 and 1996 data (Table 2). For the end of winter, we chose 10 May (day 130) for the uplands and 25 May (day 145) for the coastal plain, consistent with the nearly 2-week offset (Fig. 5) between the two provinces.

For each grid cell in the domain we implemented Eqs. (1)–(6) and the relationships in Table 4 to produce a daily record of the snow–ground interface temperature for the winter of 1994/95. Seven ''snapshots'' (Fig. 9) suggest how the interface temperature field evolved. As the winter progressed, falling air temperatures produced lower interface temperatures, which slowly pushed southward from the arctic coast. This gradual cooling

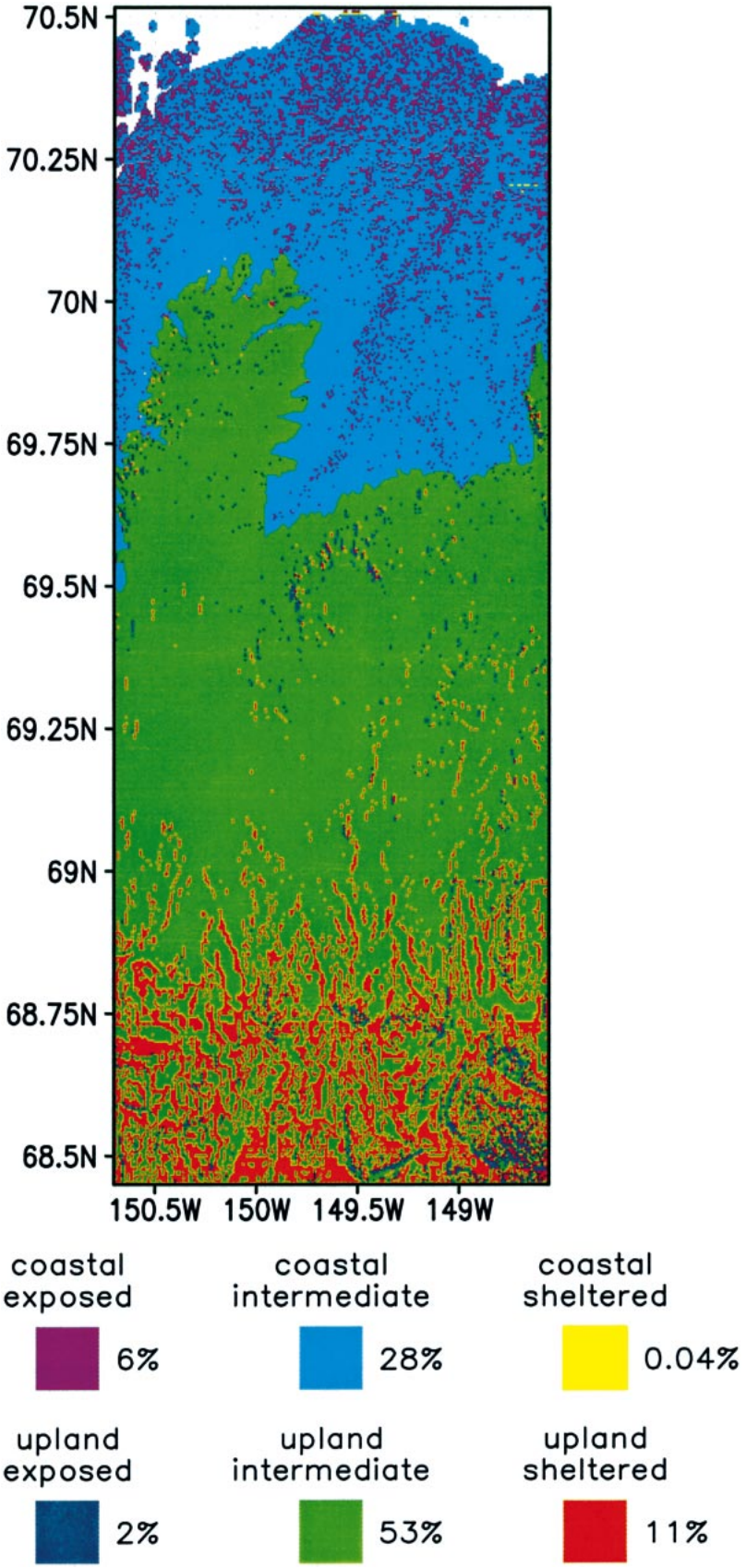

FIG. 8. The Kuparuk basin model region divided into province and exposure classes.

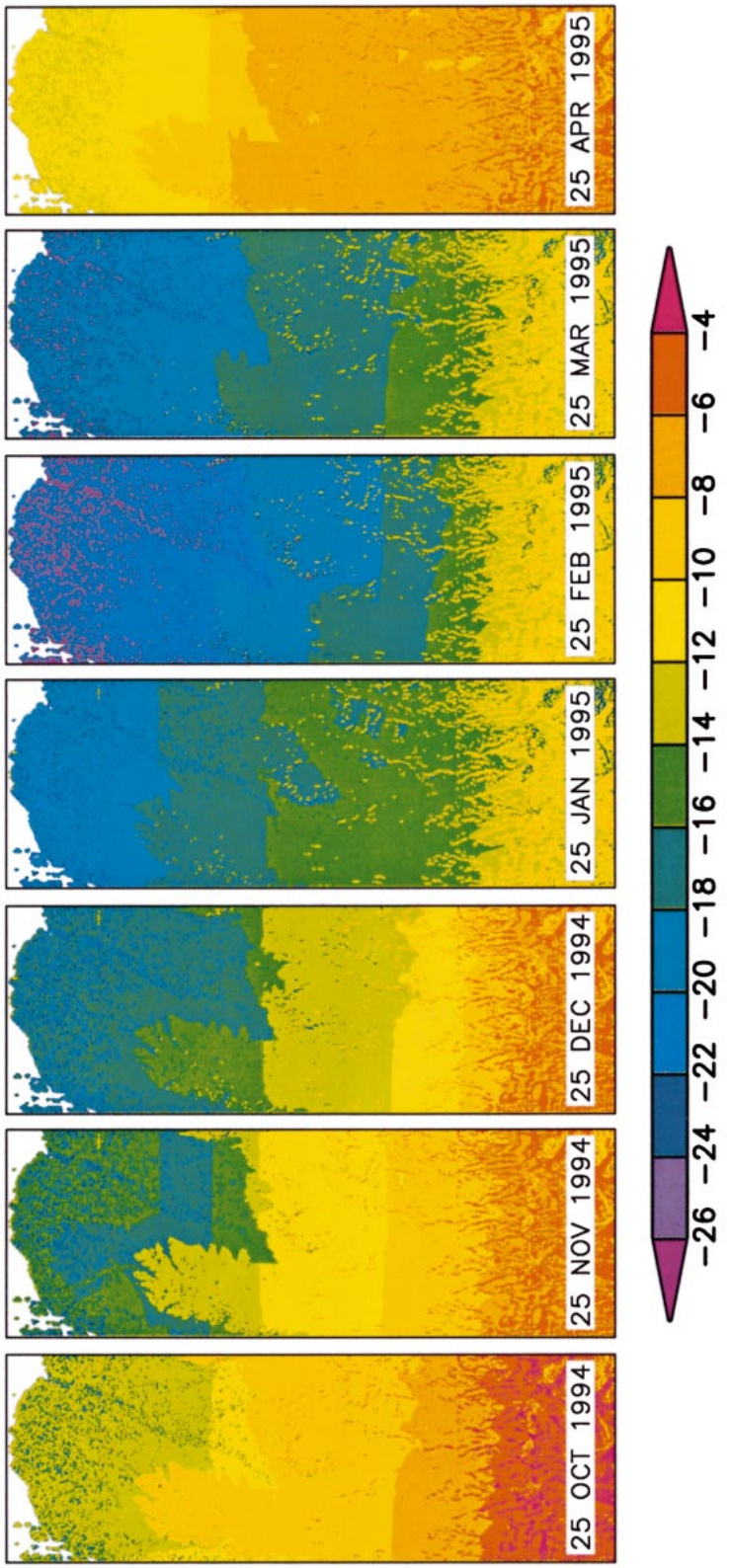

FIG. 9. Model simulations of the snow–ground interface temperature for the Kuparuk basin region, 1994/95.

between September and March was followed by a rapid, nearly synchronous warming over the entire domain in spring. Air temperature warming events propagated from south to north, while cooling events propagated from north to south. The thinner, less insulative snow of the coastal plain, coupled with this preferential movement of warming and cooling events, resulted in interface temperatures on the coastal plain that were always significantly lower than in the uplands.

The simulations indicate large spatial gradients in interface temperature that have important biological ramifications. It is known that significant winter microbial activity can take place in arctic soils and is responsible for winter CO_2 production (Kelley et al. 1968; Zimov et al. 1993a; Oechel et al. 1997; Fahnestock et al. 1998). Microbial activity is temperature-sensitive (Flanagan and Veum 1974; Nadelhoffer et al. 1991; Clein and Schimel 1995) and requires unfrozen water in the soil. Estimates vary, but, in general, activity appears to cease at temperatures lower than −6°C (Flanagan and Veum 1974; Coxson and Parkinson 1987; Zimov et al. 1993b). Above this temperature, microbial decomposition and nutrient cycling continue (Brooks et al. 1997), to the benefit of the biota. From the simulations, we mapped the number of days during the winter when the interface temperature was above this critical threshold (Fig. 10). The number of days above threshold in the underlying soil layers will be greater, depending on depth, soil moisture, and organic layer quality, but our map suggests important differences between the coastal plain and the uplands. On the coastal plain there is only a short period of time (1–4 weeks) when microbial activity at the soil surface is likely, while in the uplands this period is 2–4 times longer.

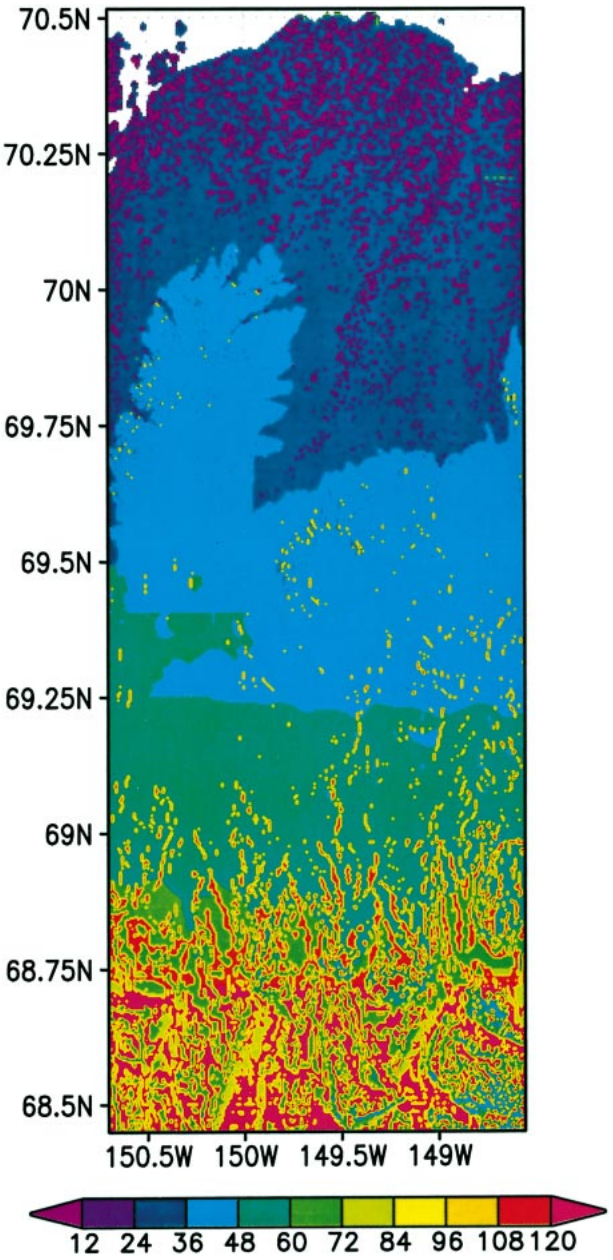

FIG. 10. Number of days when the snow–ground interface temperature is higher than −6°C based on model simulations. This is approximately the critical temperature above which microbial activity can continue.

7. Discussion

Our measurement (e.g., Figs. 1a,b) and model results (e.g., Fig. 7) show that snow cover attenuates average winter air temperature by 34%–47% (b values for relationship 1 in Table 4) and daily fluctuations in air temperature by 40%–96% (φ values for relationship 5 in Table 4). This significant moderation of frigid temperatures by the snow is critical to the ecology and biology of the vegetation and underlying soils of arctic Alaska. The full ramifications of this thermal protection are perhaps best illustrated in Fig. 6. This figure not only documents that in uplands–sheltered locations the interface temperature is nearly decoupled from air temperature, it also shows that when the interface temperature is decoupled it is nearly at the critical value for soil biological activity (−6°C). Beneath the interface, temperatures are higher and it is reasonable to assume that biological activity continues throughout the winter. One implication is that, without any change in winter air temperature, an increase in snow depth could radically change the nature of winter biological activity in the Kuparuk basin, particularly if snow depths were to exceed 80 cm.

Of course, snow is not the only factor affecting winter soil temperatures. Soil moisture and organic layer thickness play an important role as well. The soil moisture, particularly for the wet soils found in arctic Alaska, provides a store of latent heat that can significantly delay the cooling of the soil in the early part of the winter, directly affecting the snow–ground interface temperature. Organic layers, especially the mosses found in tun-

dra, provide insulation that can, when dry, equal that of the overlying snowpack [compare results from Hinzman et al. (1991, their Fig. 12) with those of Sturm et al. (1997, their Fig. 6)]. While this fine insulation does not directly affect the interface temperature, it does have a marked effect on the temperature of the underlying soil layers, protecting them about as well as the snow.

The coastal province contains a considerably higher percentage of wet tundra soils than the uplands (Walker 1995; Walker et al. 1998), and it is there we would expect the latent heat effect to be most prevalent. In fact, we see this in our data. For the nine coastal intermediate sites plotted in Fig. 6 (black diamonds with open centers), six were located in very wet tundra (Table 1, last column) and three were in drier tundra. The dry sites ranged from 2° to 5°C colder than the wet sites (appendix B), and examination of the daily data confirms that much of the difference accrued in early winter when the soil moisture was still freezing. Thick and dry (in winter) organic layers, particularly mosses, are more prevalent in the uplands (Walker 2000). We can approximate their maximum effect by assuming that they have the same insulating power as an equal thickness of snow. From Fig. 4, a 15-cm increase in snow depth produces anywhere from a 0.5° to 3°C increase in interface temperature. Fifteen centimeters is a fairly thick moss layer, and it would need to have a low moisture content (<10%; Hinzman et al. 1991) to achieve this level of thermal protection. The two effects (soil moisture and organic layer) appear to be about the same magnitude, but one (soil moisture) is already in our model (crudely) because it affected the observed interface temperatures on which the model is based, while the other (moss/organic insulation) is not. Figure 10 is therefore likely to underestimate the contrast between the coastal and uplands provinces. If anything, soil biological activity is even more viable in the uplands than on the coast and takes place over a much greater period of the winter.

But the main limitation on the accuracy of our modeling is determining the snow depth. Arctic snow is redistributed by the wind with significant variations in depth over distances as short as a few meters. Prediction of snow depth at this fine scale is not currently possible, yet this is the scale of variation that affects interface temperatures. An example of our inability to resolve these small-scale variations in depth can be seen in Fig. 8, where on the coastal plain the percentage of the sheltered snow class is unrealistically low because our DEM did not resolve the relevant topography [i.e., the river and stream cutbanks where large drifts form (Sturm et al. 2001)].

The type of model used for prediction or simulation is less important than accurately extrapolating snow depth and other atmospheric forcing fields over a domain. In fact, at the scale of the Kuparuk basin, few models can be purely physical or statistical, and the division between the two becomes fuzzy. While the basic underpinning of our model is a series of empirical regression equations, physical considerations constrain the model as well. For example, the statistics for the sheltered exposure class indicate a constant value for T_i (Table 4, relationship 1), but we could have inferred the same from the fact that, above a critical snow depth, T_i is decoupled from depth (Fig. 4). Similarly, we know from observations that the snow cover in exposed areas on the coastal plain is much like the snow cover in exposed areas in the uplands, so we use similar regression equations for both. Physical models use empirical or statistical relationships when the physics is either too obscure or too elaborate to be dealt with explicitly. We think that the challenge is, and will remain for the future, creating reliable input fields for heterogeneous systems like the Kuparuk basin, whether they drive physical, statistical, or empirical models.

8. Conclusions and model application

Using an extensive set of air and snow–ground interface temperature data from arctic Alaska, we have developed a statistical model that can simulate the interface temperature over a large domain with daily or more frequent resolution. The data show that in arctic Alaska there are two distinct winter thermal provinces (coastal and uplands) in which each of three snow exposure classes (exposed, intermediate, and sheltered) can be defined. For each province–class combination, temporal and spatial interface temperature patterns are statistically distinct. These differences were captured by defining a beta curve for each province–class combination. Beta curves are well-known statistical distributions that are able to match the key features of the temporal evolution of the interface temperature under a wide variety of conditions. Tests of the model within and outside the domain in which it was developed indicate a spatial–temporal accuracy of ±2°C when simulating average winter interface temperatures and ±3°C when simulating daily interface temperatures. The model is relatively easy to apply and requires a simpler set of gridded input data than most comparable physical models.

The model can be used to address a number of biophysical issues in arctic Alaska related to plants, animals, or the soil beneath the snow. Being able to predict the interface temperature eliminates the need for modeling the snow cover, which has traditionally proven difficult. For example, we have used the model to determine how many days during the winter the interface temperature is greater than −6°C over a domain of 20 000-km^2. This is the approximate temperature threshold below which microbial activity ceases and winter production of CO_2 stops. Our results suggest that the uplands provide a distinctly more favorable environment for winter soil biological activity than does the coastal plain. More extensive or complete models of microbial activity and decomposition could be readily driven by

our model output. Similarly, ground-freezing models or assessment of subnivian environmental stresses could be coupled to our model. The model's simplicity lends itself to this type of cross-disciplinary use.

Acknowledgments. We wish to thank Jon Holmgren, Eric Pyne, Dick Flaherty, Bert Yankielun, Martin Wilmking, and Max König for assistance in the field. Joe McFadden and Lori Quakenbush provided helpful comments on the work and its biological significance. Doug Kane, Dennis Lettenmaier, and two anonymous referees provided comments that improved the manuscript. This study was supported by National Science Foundation Grants OPP-9732007 and OPP-9415386.

APPENDIX A

List of Symbols

t	Time
t^*	Time (nondimensional)
$T_a(t)$	Air temperature
$T_i(t)$	Snow–ground interface temperature
$T_{a,\text{core}}$	Average core winter air temperature
$T_{i,\text{core}}$	Average core winter interface temperature
SD	Standard deviation
$SD_{a,\text{core}}$	Standard deviation of air temperature, core winter
$SD_{i,\text{core}}$	Standard deviation of interface temperature, core winter
$\hat{\theta}_i$	Seasonal trend of interface temperature estimated using the beta curve
$\hat{\theta}_{i,\text{resid}}$	Interface temperature estimated using the beta curve with residual temperatures applied
ε_a	Residual temperature
r	Correlation coefficient
Γ	Gamma function
φ	Residual temperature damping factor, $[SD_{i,\text{core}}/SD_{a,\text{core}}]$
α	Beta-curve fitting parameter
β	Beta-curve fitting parameter
γ	Scale parameter, air temperature, equals $-\overline{T}_a$
M	Beta-curve mode, defined as $[\{\alpha - 1\}/\{\alpha + \beta - 2\}]$
S	Beta-curve coefficient of skew, defined as $[\{2(\beta - \alpha)(\alpha + \beta + 1)^{0.5}\}/\{(\alpha + \beta + 2)(\alpha\beta)^{0.5}\}]$

In text, overbars indicate average values; carets (ˆ) indicate predicted values.

APPENDIX B

Complete and Core Winter Average Temperatures

		Complete winter*				Core winter**			
		Interface temperature		Air temperature		Interface temperature		Air temperature	
Winter	Station	Mean (°C)	SD (°C)	Mean (°C)	SD (°C)	Mean (°C)	SD (°C)	Mean (°C)	SD (°C)
1993/94	Imnav1	−7.6	4.7	−14.4	10.3	−11.7	2.8	−19	10.4
1994/95	1	—	—	−18.7	11.7	—	—	−22.1	11.8
	2	−15.6	5.6	−17.8	11.6	−18.7	5.8	−21.1	11.4
	3	−8.7	2.6	−19	12.4	−10.1	1.9	−22.5	12.3
	4	—	—	−17.9	12.2	−12.9	2.8	−21.7	11.7
	5	−5.2	2.3	−19.2	12.4	−6.8	2	−22.6	12.3
	6	−9.2	3.3	−18	12.2	−11.9	1.8	−21.5	11.9
	7	−7.3	2.8	−20.3	12.3	−7.1	2.2	−23.1	12.1
	8	−10.4	3.3	—	—	−12.9	2.1	−24.1	12.1
	9	−5.5	1.2	−21.2	12.1	−5.8	0.7	−24.4	11.9
	10	−12.6	3.4	−19.5	12.2	−14.8	2.1	−23.1	11.8
	11	−14.5	4.5	−20.4	11.4	−17	3.8	−23.6	11.6
	12	−12.3	4.2	−20.3	11.8	−15.3	2.5	−24	11.4
	13	−19.5	6.7	—	—	−21.4	7	−25.3	11.7
	14	−14.1	4.8	−22.4	11.8	−17.8	3.1	−26.3	10.9
	14.5	—	—	—	—	—	—	—	—
	15	−8.9	2.2	—	—	−10.4	1.4	−26.6	10.5
	16	—	—	—	—	−15.4	1.7	−25.4	10.6
	17	−17.1	5.7	−20.7	11.5	−20.3	4.6	−24.8	10.6
	18	−20.9	6.3	−23.2	9.5	−23.5	6.4	−25.6	10.6
	19	−14.2	5.2	−22.3	11.5	−18.3	3	−26.5	10.4
	20	—	—	—	—	−20.1	3	−28.5	10
	21	−16.3	6.1	—	—	−20.6	3.2	−28.8	9.9
	22	−12.1	4.2	−24	10.8	−14.3	2.7	−26.9	10
	23	−17.3	6.6	−21.8	11.9	−22.1	3.4	−28.7	9.9
	24	—	—	−21.6	12	−19	2.2	−28.7	9.9
	25	−16	6.3	—	—	−20.8	3.4	—	—
	26	—	—	−22	11.9	−24.2	6.2	−28.9	9.7

APPENDIX B
(*Continued*)

		Complete winter*				Core winter**			
		Interface temperature		Air temperature		Interface temperature		Air temperature	
Winter	Station	Mean (°C)	SD (°C)	Mean (°C)	SD (°C)	Mean (°C)	SD (°C)	Mean (°C)	SD (°C)
	27	—	—	—	—	−18.7	2.3	−28.9	9.8
	28	−15.2	5	−21.5	12	−19	2.3	−28.7	9.8
	29	—	—	—	—	−18	3	−27.8	9.7
	30	−15.9	4.9	−21.5	11.8	−19.4	1.9	−28.8	9.6
	Imnav2	−6.8	3.7	−14.2	10.6	−10.4	2	−19.4	11
Averages	Whole basin	−12.8	4.4	−20.3	11.7	−16.2	3	−25.3	10.9
	Uplands	−11.9	4	−19.7	11.7	−14.3	3	−23.7	11.4
	Coastal	−15.5	5.5	−22.1	11.7	−19.6	3.1	−28.5	9.8
1995/96	1	—	—	—	—	—	—	−17.8	11
	2	−12.6	6.4	−16.6	9.4	−17.2	6	−17.8	10.7
	3	—	—	—	—	−7.7	1.3	—	—
	4	—	—	—	—	−12	2.9	−18.1	10.6
	6	—	—	−16.4	10	—	—	−18.2	10.6
	9	−8.2	2.9	—	—	−8	1	−21.3	11.8
	10	—	—	—	—	−12.7	1.7	−18.6	10.6
	11	−10.4	3.8	−17.7	10	−13.1	2.3	−19	10.9
	14	−10.6	5.1	−19.1	12.3	−14.1	2.3	−21.6	11.3
	14.5	−12.9	5.3	−20.8	11.8	−16.3	2.9	−22	12.4
	Imnav1	−4.3	1.5	−14.6	9.2	−5.5	0.6	−17.7	10.1
	Imnav2	−8.4	3.6	−14.6	9.2	−11.4	2.7	−17.7	10.1
Averages	Uplands	−9.6	4.1	−17.1	10.3	−11.8	2.4	−19.1	10.9

* Complete winter air temperatures (mean and SD) are truncation corrected for 1995/96 only.
** Core winter air temperatures (mean and SD) are truncation corrected.

REFERENCES

Adams, W. P., and N. T. Roulet, 1982: Areal differentiation of land and lake snowcover in a small sub-arctic drainage basin. *Nord. Hydrol.,* **13,** 139–156.

Anderson, E. A., 1976: A point of energy and mass balance model of a snow cover. National Weather Service, Office of Hydrology Tech. Rep. PB-254-653, 151 pp.

Benson, C. S., 1969: *The Seasonal Snow Cover of Arctic Alaska.* The Arctic Institute of North America, 47 pp.

——, and M. Sturm, 1993: Structure and wind transport of seasonal snow on the Arctic slope of Alaska. *Ann. Glaciol.,* **18,** 261–267.

Brooks, P. D., S. K. Schmidt, and M. W. Williams, 1997: Winter production of CO_2 and N_2O from alpine tundra: Environmental controls and relationship to inter-system C and N fluxes. *Oecologia,* **110,** 403–413.

Brun, E., E. Martin, V. Simon, C. Gendre, and C. Coleou, 1989: An energy and mass model of snow cover suitable for operational avalanche forecasting. *J. Glaciol.,* **35,** 333–342.

Clein, J. S., and J. P. Schimel, 1995: Microbial activity of tundra and taiga soils at sub-zero temperatures. *Soil Biol. Biochem.,* **27,** 1231–1234.

Coxson, D. S., and D. Parkinson, 1987: The pattern of winter respiratory response to temperature, moisture, and freeze-thaw exposure in *Bouteloua gracilis* dominated grassland soils of southwestern Alberta. *Can. J. Bot.,* **65,** 1716–1725.

Desrochers, D. T., and H. B. Granberg, 1988: Schefferville snow–ground interface temperatures. *Permafrost, 5th International Conference Proceedings.* K. Senneset, Ed., Tapir, 67–72.

Evans, M., N. Hastings, and B. Peacock, 1993: *Statistical Distributions.* John Wiley and Sons, 169 pp.

Fahnestock, J. T., M. H. Jones, P. D. Brooks, D. A. Walker, and J. M. Welker, 1998: Winter and early spring CO_2 effluc from tundra communities of northern Alaska. *J. Geophys. Res.,* **103** (D22), 29 023–29 027.

Flanagan, P. W., and A. K. Veum, 1974: Relationships between respiration, weight loss, temperature and moisture in organic residues on tundra. *Soil Organisms and Decomposition in Tundra,* A. J. Holding et al., Eds., Tundra Biome Steering Committee, 249–277.

Hinzman, L. D., and D. L. Kane, cited 2002: Meteorological and hydrographic data, Kuparuk River watershed, 1985–1998. NSIDC–ARCSS Data and Information Archive. [Available online at http://arcss.colorado.edu/data/arcss015.html.]

——, ——, R. E. Gieck, and K. R. Everett, 1991: Hydrologic and thermal properties of the active layer in the Alaskan Arctic. *Cold Reg. Sci. Technol.,* **19,** 95–110.

——, D. J. Goering, and D. L. Kane, 1998: A distributed thermal model for calculating soil temperature profiles and depth of thaw in permafrost regions. *J. Geophys. Res.,* **103** (D22), 28 975–28 991.

IASH, 2001: Global water data: A newly endangered species. *EOS, Trans. Amer. Geophys. Union,* **82,** p. 54, 56, and 58.

Jordon, R., 1991: A one-dimensional temperature model for a snow cover. U.S.A. CRREL Rep. 91-16.

Kelley, J. J., D. F. Weaver, and B. P. Smith, 1968: The variation of carbon dioxide under the snow in the arctic. *Ecology,* **49,** 358–361.

König, M., and M. Sturm, 1998: Mapping snow distribution in the Alaskan Arctic using aerial photography and topographic relationships. *Water Resour. Res.,* **34,** 3471–3483.

Liston, G. E., and M. Sturm, 1998: A snow-transport model for complex terrain. *J. Glaciol.,* **44,** 498–516.

Nadelhoffer, K. J., A. E. Giblin, G. R. Shaver, and J. A. Laundre, 1991: Effects of temperature and substrate quality on element mineralization in six arctic soils. *Ecology,* **72,** 242–253.

Nelson, F. E., S. I. Outcalt, K. M. Hinkel, and B. M. Murray, 1988: Microtopographic thermal contrasts, northern Alaska. *Permafrost, 5th International Conference Proceedings,* K. Senneset, Ed., Tapir, 819–823.

——, N. I. Shiklomanov, G. R. Mueller, K. M. Hinkle, D. A. Walker, and J. G. Bockheim, 1997: Estimating active-layer thickness over

a large region: Kuparuk River Basin, Alaska, U.S.A. *Arct. Alp. Res.,* **29,** 367–378.

Neter, J., W. Wasserman, and M. H. Kutner, 1990: *Applied Linear Statistical Models: Regression, Analysis of Variance, and Experimental Design.* Irwin, 1181 pp.

Oechel, W. C., G. L. Vourlitis, and S. J. Hastings, 1997: Cold-season CO_2 emission from arctic soils. *Global Biogeochem. Cycles,* **11,** 163–172.

Pomeroy, J. W., and D. M. Gray, 1995: *Snowcover Accumulation, Relocation and Management.* National Hydrology Research Institute, 144 pp.

Smith, M. W., 1975: Microclimatic influences on ground temperatures and permafrost distribution, MacKenzie Delta, Northwest Territories. *Can. J. Earth Sci.,* **12,** 1421–1438.

Sturm, M., cited 2002: Air and ground surface temperatures from the Kapurak basin, Alaska, 1994–1996. NSIDC–ARCSS Data and Information Archive. [Available online at http://arcss.colorado.edu/data/arcss001.html.]

——, and J. Holmgren, 1994: Effects of microtopography on texture, temperature and heat flow in arctic and sub-Arctic snow. *Ann. Glaciol.,* **19,** 63–68.

——, ——, and G. E. Liston, 1995: A seasonal snow cover classification system for local to global applications. *J. Climate,* **8,** 1261–1283.

——, ——, M. Konig, and K. Morris, 1997: The thermal conductivity of seasonal snow. *J. Glaciol.,* **43,** 26–41.

——, G. E. Liston, C. S. Benson, and J. Holmgren, 2001: Characteristics and growth of a snowdrift in arctic Alaska, U.S.A. *Arct. Antarct. Alp. Res.,* **33,** 319–329.

Wahrhaftig, C., 1965: Physiographic divisions of Alaska. U.S. Geological Survey Prof. Paper 482, 52 pp.

Walker, D. A., 1995: Toward a new circumpolar arctic vegetation map: St Petersburg Workshop. *Arct. Alp. Res.,* **31,** 169–178.

——, 2000: Hierarchical subdivision of arctic tundra based on climate, parent material, and topography. *Global Change Biol.,* **6,** 19–34.

——, cited 2002: GIS data from the Alaska north slope. Kapurak River basin 1:250 000 scale map of land cover. NSIDC–ARCSS Data and Information Archive. [Available online at http://nsidc.org/data/arcss015.html.]

——, K. R. Everett, P. J. Webber, and J. Brown, 1980: *Geobotanical Atlas of the Prudhoe Bay Region, Alaska.* U.S. Army Cold Regions Research and Engineering Laboratory Rep. 80-14, 69 pp.

——, and Coauthors, 1998: A major arctic soil pH boundary: Implications for energy and trace-gas fluxes. *Nature,* **394,** 469–472.

Walker, M. D., D. A. Walker, and N. A. Auerbach, 1994: Plant communities of a tussock tundra landscape in the Brooks Range Foothills, Alaska. *J. Veg. Sci.,* **5,** 843–866.

Whiteman, C. D., J. M. Hubbe, and W. J. Shaw, 2000: Evaluation of an inexpensive temperature datalogger for meteorological applications. *J. Atmos. Oceanic Technol.,* **17,** 77–81.

Zimov, S. A., I. P. Semiletov, S. P. Daviodov, I. V. Voropaev, S. F. Prosyannikov, C. S. Wong, and Y. H. Chan, 1993a: Wintertime CO_2 emission from soils of northeastern Siberia. *Arctic,* **46,** 197–204.

——, G. M. Zimova, S. P. Daviodov, A. I. Daviodova, Y. V. Voropaev, Z. V. Voropaeva, S. F. Prosiannikov, and O. V. Prosiannikova, 1993b: Winter biotic activity and production of CO_2 in Siberian soils: A factor in the greenhouse effect. *J. Geophys., Res.,* **98,** 5017–5023.